Journal of Power Sources 230 (2013) 321–326

Contents lists available at SciVerse ScienceDirect

Journal of Power Sources

journal homepage: www.elsevier.com/locate/jpowsour

Short communication

Preparation and characterization of porous Nb_2O_5 photocatalysts with CuO, NiO and Pt cocatalyst for hydrogen production by light-induced water splitting

Yi-Hao Pai*, Su-Yun Fang

Department of Opto-Electronic Engineering, National Dong Hwa University, No. 1, Sec. 2, Da Hsueh Rd., Shoufeng, Hualien 97401, Taiwan, ROC

HIGHLIGHTS

- The oxidation temperature plays an important role in porous Nb_2O_5 matrix formation.
- The presence of the Nb_2O_5 with CuO cocatalyst can promote the H_2 production rate.
- CuO cocatalyst can substitute noble metals in photocatalysts for H_2 production.
- The use of porous CuO/Nb_2O_5 photocatalyst can inhibit CO poisoning.
- The porous CuO/Nb_2O_5 photocatalyst can effectively maintain the catalyst activity.

ARTICLE INFO

Article history:
Received 24 September 2012
Received in revised form
10 December 2012
Accepted 13 December 2012
Available online 27 December 2012

Keywords:
Hydrogen production
Photocatalysts
Niobium pentoxide
Photoelectrochemistry

ABSTRACT

In this study, porous Nb_2O_5 photocatalyst materials are prepared through thermal oxidation. According to X-ray photoelectron spectroscopy (XPS), at a temperature of 500 °C, an optimum porous Nb_2O_5 photocatalyst is obtained with an O/Nb ratio close to the theoretical value of 2.5. The X-ray powder diffractometer (XRD) result shows that at the main diffraction angles of 22.63° and 28.33°, crystalline diffraction signals of Nb_2O_5 appear with corresponding diffraction planes of (001) and (180). When CuO, NiO and Pt catalysts are added to Nb_2O_5 as the cocatalyst for comparison, the maximum hydrogen production efficiency for a CuO/Nb_2O_5 photocatalyst is achieved (1405 μmol h^{-1} g^{-1}). However, when NiO and Pt are added as cocatalysts, the hydrogen production efficiencies are decreased to 800 μmol h^{-1} g^{-1} and 510 μmol h^{-1} g^{-1}, respectively. Through the photoelectrochemical analysis, it finds that the CO signal peak with incomplete oxidation significantly increases as the reaction time increases, thus causing CO to adsorb on the catalyst surface (such as NiO or Pt) leading to catalyst poisoning. This results in reduced catalyst performance and hydrogen production rates.

1. Introduction

In recent years, greenhouse gas emissions from fossil fuels have worsened the greenhouse effect and created a serious impact on the environment. Hence, seeking alternative fuels and environmentally friendly green energy technologies has become a major concern. In particular, the development of hydrogen energy technology achieved a breakthrough in 1972. The key lies in the use of semiconductor catalysts in water-splitting hydrogen production under ultraviolet irradiation, which makes solar hydrogen production applications more feasible [1]. When choosing semiconductor catalysts used in hydrogen production, the key lies in the selection of photocatalyst materials. Transition element metal oxides with d^0 or d^{10} electronic configuration can split water into H_2 and O_2 due to high photochemical activity [2]. Among the many semiconductor materials, applications of Nb_2O_5 have become widely prevalent [4] due to their unique physical properties such as a high refractive index, a wide bandgap (3.1–3.5 eV), good chemical and thermal stability [3] and good photocatalytic characteristics. In publications we find that the addition of metal particles (Pt, Au) or metal oxides (NiO, RuO_2) into semiconductor materials can delay electron and hole recombination rates, quickly export electrons and promote reduction reaction, thereby enhancing quantum efficiency [5–7]. Kudo et al. proposed that $NaTaO_3$ doped with 2 mol% La and modified by a NiO cocatalyst under ultraviolet irradiation can enhance the efficiency of water-splitting hydrogen production [6]. Lin et al. prepared a catalyst containing Nb_2O_5 and added metal particles, such as Pt and Au, to study the photochemical hydrogen production. The results show that the addition of metal particles or

* Corresponding author. Tel./fax: +886 3 8634195.
E-mail addresses: paiyihao@mail.ndhu.edu.tw, paiyihao@gmail.com (Y.-H. Pai).

0378-7753/$ – see front matter © 2012 Elsevier B.V. All rights reserved.
http://dx.doi.org/10.1016/j.jpowsour.2012.12.078

metal oxides into the photocatalyst materials effectively enhanced the catalyst activity and hydrogen production efficiency [7]. Additionally, it pointed out that the use of ultraviolet light sources and higher concentrations of sacrificial reagents can effectively enhance the hydrogen production rate [8–10]. However, studies on the effects of different dopants on cocatalyst materials' hydrogen production under visible light conditions showed differences in hydrogen production efficiency under low-concentration methanol solution environments, and even long-term hydrogen production assessments remained scarce.

In this study, a low-temperature thermal oxidation approach was adopted to prepare porous Nb_2O_5 photocatalyst materials. Through XPS, optimal process conditions were found. In addition, in order to further gain insights into the impact of the cocatalyst on the porous Nb_2O_5 photocatalyst materials, CuO, NiO and Pt were selected as the porous Nb_2O_5 cocatalysts. Finally, using the photochemical hydrogen production system under 300 W white light source irradiation, the photocatalysts were placed in a methanol aqueous solution (with a volume ratio of MeOH:H_2O = 1:9) to carry out hydrogen production efficiency tests and comparisons.

2. Experiment

2.1. Preparation and analysis of porous Nb_2O_5 powder

First, a sufficient amount of metal Nb powder (Alfa Aesar 99.8%) was placed in a high-temperature furnace and annealed for 1 h at 100 °C, 350 °C and 500 °C, respectively, under specific air conditions (21/79 mol% O_2/N_2). Subsequently, X-ray photoelectron spectroscopy (XPS/ESCA, Thermo K-alpha) XPS was used to establish optimal thermal oxidation temperature conditions, and the Nb_2O_{5-x} powder obtained through annealing at 200 °C, 350 °C and 500 °C underwent stoichiometry tests.

2.2. Preparation of NiO/Nb_2O_{5-x}, CuO/Nb_2O_{5-x}, and Pt/Nb_2O_{5-x} photocatalyst powder

For the Pt/Nb_2O_{5-x} photocatalyst powder, 1 g of optimized Nb_2O_{5-x} photocatalyst powder was first obtained and placed into 200 ml of methanol aqueous solution to be mixed using ultrasonic wave (100 kHz) technology. Then, an appropriate amount of $H_2PtCl_6 \cdot 6H_2O$ aqueous solution was added into the above mixed aqueous solution. Finally, the $NaBH_4$ aqueous solution was added and stirred for 20 min at room temperature to perform a reduction and obtain Pt/Nb_2O_{5-x} photocatalyst powder with 2 wt% Pt catalyst adsorption. Then, using a vacuum oven, the powder was dried completely in a vacuum at 70 °C.

For CuO cocatalyst synthesis, 1 g of optimized Nb_2O_{5-x} powder was first obtained to serve as the carrier. Then, it was placed in 200 ml of ethanol, and 2 wt% commercial nano CuO photocatalyst powder was added. At room temperature, it was stirred using ultrasonic mixing technology, and the solid participate obtained was cleaned and filtered using deionized water (DI). Then, it was backed at 70 °C in a vacuum oven to dry completely and produce CuO/Nb_2O_{5-x} photocatalyst powder. A NiO/Nb_2O_{5-x} catalyst powder was also prepared in a similar manner in accordance with the above mentioned synthesis steps.

2.3. Charactersitics and hydrogen production test of porous NiO/Nb_2O_{5-x}, CuO/Nb_2O_{5-x}, and Pt/Nb_2O_{5-x} photocatalysts

An X-ray powder diffractometer (XRD, Model No. Rigaku D/MAX-2500) was used to identify the crystal structure and composition of the prepared photocatalyst powder mentioned above. Then, using a field emission scanning electron microscope (FESEM, JEOL JSM-7000F), an accurate description was made of the surface morphology of the photocatalysts. A columnar quartz glass tank, sheathed with a cooling water circulation system, was adopted for research on hydrogen production. A 300 W white light source (Philips ELH-316190 ELH 300 W 120 V, purchased from Nano-precision Technology Co., Ltd.) was installed at the bottom of the reaction vessel mentioned above (as shown in Fig. 1(a) and (b)). A broadband light source with an output power of 50 mW cm^{-2} was applied to illuminate the photochemical cell. The photocatalyst water-splitting hydrogen production conditions necessary for photocatalytic reactions to take place include the addition of 0.2 g of photocatalyst powder into 150 ml of methanol aqueous solution at a temperature of 50 °C (the volume ratio is MeOH:H_2O = 1:9). Methanol decomposition was performed for 16 h, and the hydrogen gas evolution was determined beginning at 3 h. Finally, through the "collection of gases over water" approach, gases from the reaction were collected. The water displacement system includes a water-filled container connected to a reaction vessel and a water removal conduit. The electrochemical properties of the electrode was analyzed using a cyclic voltammetry (CV) technique through a CHI614D electrochemical analyzer, while a Pt wire served as the

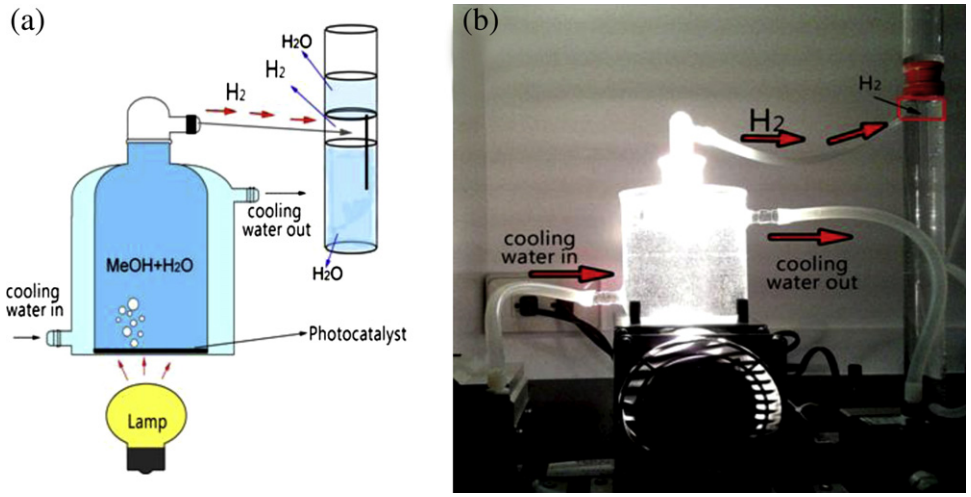

Fig. 1. (a) Scheme of closed reaction system for hydrogen production by light-induced water splitting; (b) the photoelectrolysis cell setup with a collimated light beam passed through a quartz window to illuminate a photocatalyst layer.

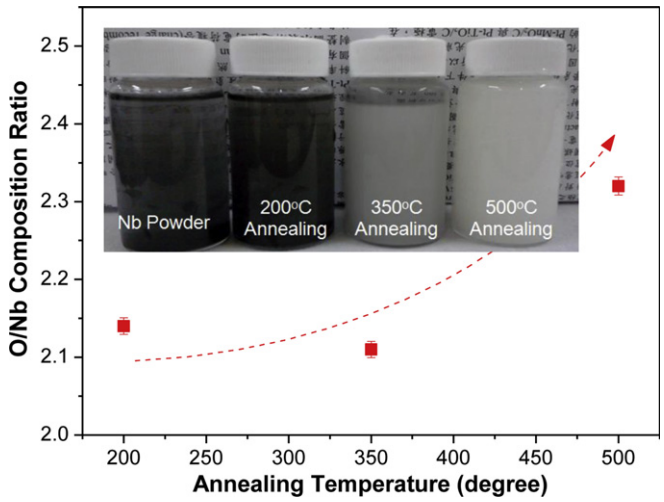

Fig. 2. An element content analysis on the Nb_2O_{5-x} photocatalyst powder prepared under different thermal oxidation temperatures. (Inset: photo images of the Nb_2O_{5-x} photocatalyst powder consisted of co-solvent.)

counter electrode and Ag/AgCl served as the reference electrode. The electrocatalytic activity of the electrodes toward electro-oxidation of methanol was examined in a deaerated aqueous solution of 1 M H_2SO_4 containing 1 M of methanol at 27 °C under 300 W white light source irradiation for about 4 cycles with a scan rate of 20 mV s^{-1}.

3. Results and discussion

3.1. The characteristics of Nb_2O_{5-x} photocatalyst powder

In order to find optimal process conditions, the XPS was first adopted in this study to conduct an element content analysis on the Nb_2O_{5-x} photocatalyst powder prepared under different thermal oxidation temperatures (200 °C, 350 °C and 500 °C), as shown in Fig. 2. The diagram shows that when the annealing temperature was below 350 °C, the O/Nb ratio was about 2.1; when the annealing temperature was increased to 500 °C, the O/Nb ratio increased significantly to 2.32. According to Fick's First Law ($D = D_0\exp(-Q/RT)$), the diffusion rate (D) and temperature (T) show a nonlinear proportional relationship [11]. Hence, under the same aerobic condition, an increase in annealing temperature accelerated the oxidation reaction, since the oxidation reaction speed of the oxide/gas interface and metal/oxide surface increased relatively in order to achieve equilibrium. Under low-temperature annealing conditions, the diffusion rate significantly decreased, thus resulting in changes in the oxidation state. Possible oxidation equations are $2Nb + O_2 \rightarrow 2NbO$ and $2NbO + O_2 \rightarrow 2NbO_2$. Note that niobium forms oxides with oxidation states from +2 (NbO)

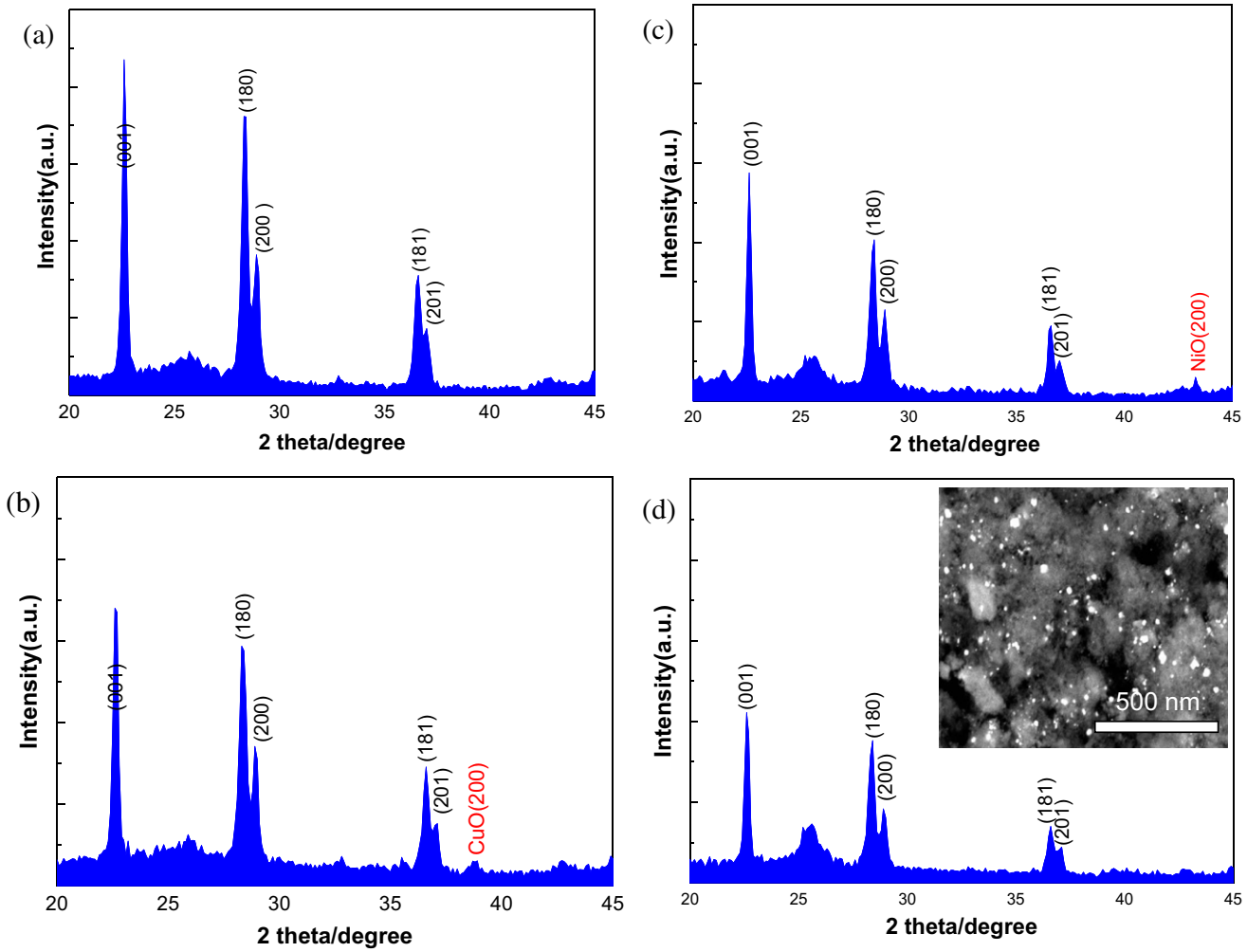

Fig. 3. The wide angle XRD spectra of the (a) Nb_2O_5, (b) CuO/Nb_2O_5, (c) NiO/Nb_2O_5, and (d) Pt/Nb_2O_5 powder (Inset in (d): the backscatter electron image of the Pt/Nb_2O_5 photocatalyst).

to +5 (Nb_2O_5) when the annealing temperature as well as the diffusion rate are increased. The pentoxide state is the most frequently encountered [12]. In addition, most metal oxide growth rates are diffusion-controlled. According to studies by Lim and Choi, oxygen concentration in the preparation process affected the oxidation reaction process of Nb [13]. Therefore, in order to effectively obtain a stable Nb_2O_5 crystal phase, the thermal oxidation temperature and oxygen supply are considered extremely important.

Overall, when the temperature is 500 °C, the O/Nb ratio is closer to the theoretical value for Nb_2O_5 of 2.5. In addition, a comparison of the photos of the paste aqueous solution prepared from powder shows that in terms of external color changes, the metal Nb powder was black at 200 °C thermal oxidation and gray at 350 °C. When the thermal oxidation temperature was increased to 500 °C, it became milky white in color. To recap, as the thermal oxidation temperature increased, the color of the Nb powder gradually turned from black gray to milky white.

3.2. The characteristics of the cocatalyst mixed with the Nb_2O_{5-x} photocatalyst powder

Fig. 3 shows the wide-angle X-ray diffraction pattern of the photocatalyst powders (CuO/Nb_2O_{5-x}, NiO/Nb_2O_{5-x} and Pt/Nb_2O_{5-x}) synthesized using Nb_2O_{5-x} powder after thermal oxidation treatment at 500 °C with the addition of cocatalysts. According to the standard diffraction pattern JCPDS Card (27-1003, 45-0937, 47-1049 and 04-0802), the comparison of Fig. 3(a)–(d) shows that at main diffraction angles of 22.63° and 28.33°, crystalline diffraction signals of Nb_2O_5 appeared, and the corresponding diffraction planes were (001) and (180). In addition, the preferred orientation of the crystal was Nb_2O_5 (001). When the photocatalyst powder synthesized with the addition of a CuO cocatalyst at a diffraction angle of 38.96°, the diffraction surface of CuO(200) was found (Fig. 3(b)). In Fig. 3(c), the diffraction signal at the location of 43.28° corresponded to the crystal signals of NiO (200). Based on Fig. 3(d), no apparent Pt diffraction signal was found; one can assume this was because of its nanoscale and location on the photocatalyst surface. This phenomenon can be attributed to the nano phenomenon produced during the bottom-up synthesis process [14]. In more detail, the amount and scale of Pt nanodots are so few and so small that the nanodots cannot produce strong diffraction. Furthermore, a weak broad amorphous feature of the glass holder appears around 39°, leading to the screening of weak diffraction intensity of the Pt nanodots [15]. To obtain further proof, verifications were made through a backscatter electron image (BEI) from a field-emission scanning electron microscope (Fig. 3(d) illustration) [16]. The average particle size ranged from a few nanometers to tens of nanometers. In order to further observe the morphology of the photocatalysts, the surface structure was

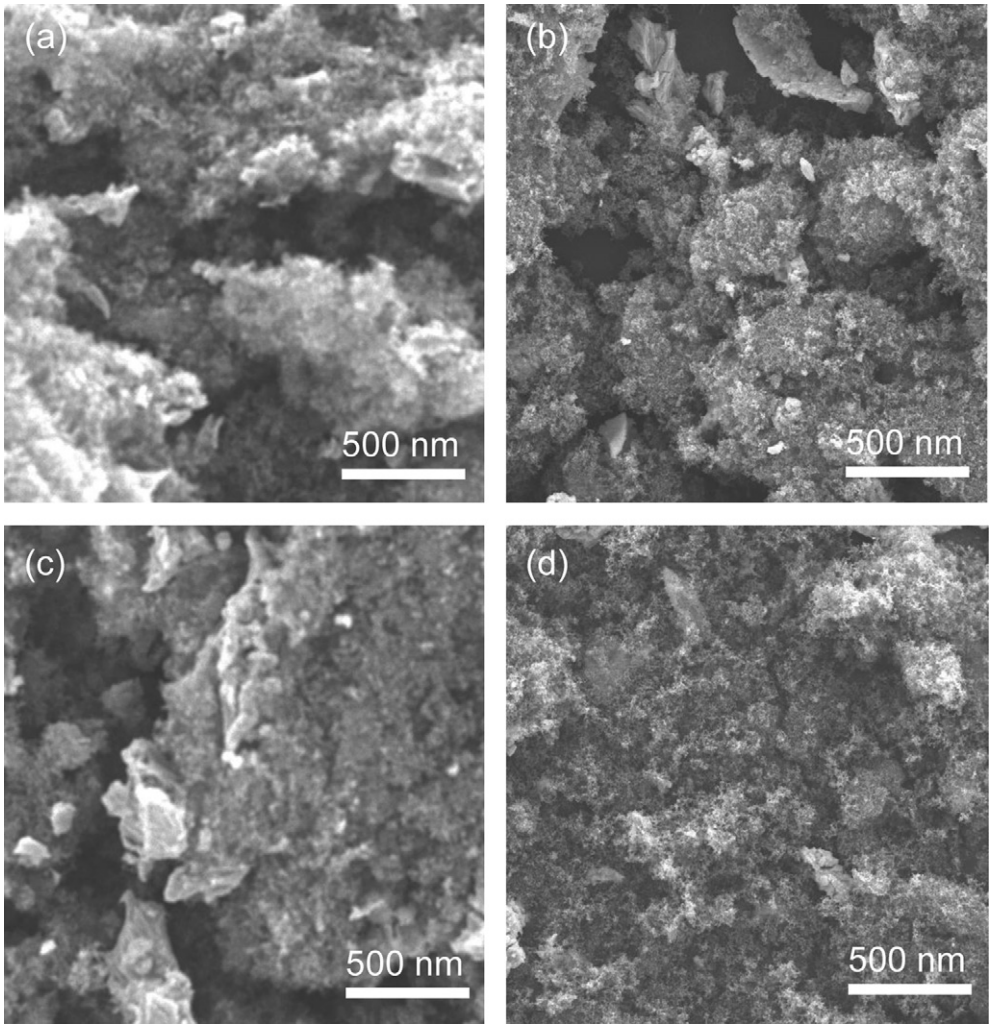

Fig. 4. The SEM images of the (a) Nb_2O_5, (b) CuO/Nb_2O_5, (c) NiO/Nb_2O_5, and (d) Pt/Nb_2O_5 photocatalyst.

observed using a scanning electron microscope, as shown in Fig. 4. Fig. 4 indicates that all four photocatalysts of Nb_2O_5, CuO/Nb_2O_5, NiO/Nb_2O_5 and Pt/Nb_2O_5 had porous structures, especially the plush-like organization surface structure of Pt/Nb_2O_5 prepared using the bottom-up synthesis method; this indicates its higher surface area.

3.3. The photo-dissolution hydrogen production and photoelectrochemistry of bicomponent photocatalysts

To further explore the actual hydrogen production efficiency of the four types of photocatalysts, a photochemical hydrogen production system was subsequently adopted in this study. In an aqueous solution environment using methanol as the sacrificial reagent, the hydrogen production efficiency was measured, as shown in Table 1. Note that the most common examples of hole scavenging agents introduced into a solution are alcohols (usually methanol), amines (such as triethanolamine or EDTA) or sulfite salts. Among them, methanol has been widely used for photodecomposition for water splitting, since the decomposition energy for methanol is 0.7 eV, which is a lower splitting energy than water [17,18]. Note that the energy of the absorbed photon must be at least 1.23 eV for water-splitting [19]. Methanol was added to water as a strong oxidation agent. In particular, methanol is used here to efficiently separate the hole-charges, which leads to a reduction in the hole–electron pair recombination process. Under the same test conditions, without the addition of any cocatalysts, the hydrogen production efficiency of Nb_2O_5 photocatalyst material was 1120 μmol h^{-1} g^{-1}. After adding CuO as the cocatalyst, the hydrogen production rate reached a maximum value of 1405 μmol h^{-1} g^{-1}. Yu et al. reported the possibility of using CuO-modified TiO_2. The optimal CuO content was found to be 1.3 wt%, creating a maximum hydrogen production rate of 2061 μmol h^{-1} g^{-1} [20]. Our optimal results are similar to those observed on a CuO-modified host matrix as a substitute for noble metals in photocatalytic hydrogen production. According to the publication, methanol decomposition in catalysts consists of three steps: (1) methanol undergoes adsorption and dissociation to become a surface methoxy group and hydrogen; (2) the methoxy group further undergoes dehydrogenation to form CO and (3) CO and hydrogen undergo desorption [21]. CuO is the activity center of CO oxidation, and the introduction of CuO makes CO re-oxidation easier, thereby enhancing the catalyst's resistance to CO poisoning [22,23]. Liu et al. also reported that the activity and selectivity for preferential oxidation of CO to CO_2 can be strongly enhanced by dispersing the CuO well at a low temperature [24]. When NiO was added as the cocatalyst, the hydrogen production efficiency dropped to 800 μmol h^{-1} g^{-1}; when Pt was added as the cocatalyst, the hydrogen production efficiency was only 510 μmol h^{-1} g^{-1}. These results can be attributed to methanol having a tendency to adsorb on the catalyst surface and produce CO to adsorb on the cocatalyst surface through a reaction equation (cocatalyst + CH_3OH → cocatalyst-CO_{ad} + 4 H^+ + 4 e^-). In other words, when these cocatalysts are deprived of the ability to oxidize CO (e.g. Pt or NiO), they become highly adsorptive to CO and desorption becomes unlikely (e.g. the adsorption force between CO and Pt is about 180 kJ mol^{-1}) [25,26]. Therefore, the photocatalyst surface becomes occupied by CO and the active position of catalytic reactions gradually decreases, thus leading to reduced hydrogen production

Table 1
The hydrogen production efficiency of Nb_2O_5, CuO/Nb_2O_5, NiO/Nb_2O_5, and Pt/Nb_2O_5 photocatalyst by light-induced water splitting.

Nb_2O_5	CuO/Nb_2O_5	NiO/Nb_2O_5	Pt/Nb_2O_5
1120 μmol h^{-1} g^{-1}	1405 μmol h^{-1} g^{-1}	800 μmol h^{-1} g^{-1}	510 μmol h^{-1} g^{-1}

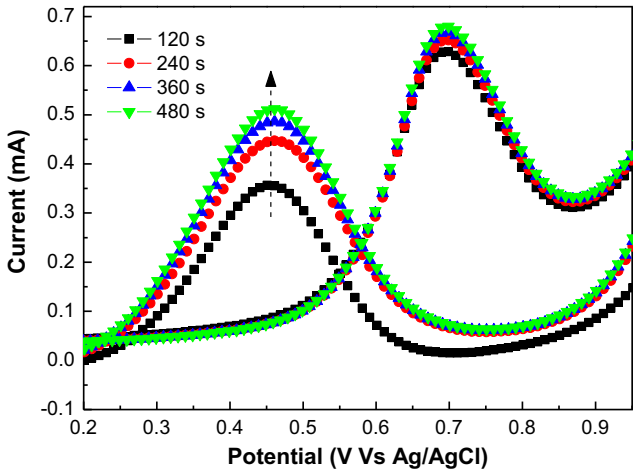

Fig. 5. The reaction time dependent CVs for methanol electro-oxidation at Pt/Nb_2O_5 electrodes in 1 M HSO_4 containing 1 M methanol (Potential scan rate: 20 mV s^{-1}).

efficiency. Hence, electro-oxidation and electro-catalytic diagnosis were further conducted through an electrochemical analyzer targeting the Pt/Nb_2O_5 photocatalyst in methanol aqueous solution (1 M of H_2SO_4 deoxy-aqueous solution mixed with 1 M of methanol), as shown in Fig. 5. The diagram shows that methanol oxidation peak signals appeared in the Pt/Nb_2O_5 photocatalyst from 0.6–0.8 V. During the reverse scanning process, the apparent signal peaks appeared near 0.45 V. These results can be attributed to the incomplete oxidation of methanol during the oxidation process, and thus, the adsorption to CO or other intermediates on the catalyst metal surface [27]. In particular, the signal peaks clearly showed an upward trend with a longer reaction time. This finding signifies that CO or other intermediates continued to accumulate on the catalyst surface and cause catalyst poisoning, thus depriving the catalyst of the methanol reaction activity center and decreasing the catalytic performance and hydrogen production rate.

4. Conclusions

A low-temperature thermal oxidation approach was adopted to prepare the porous Nb_2O_5 photocatalyst materials. XPS results pointed out that at a temperature of 500 °C, the optimized porous Nb_2O_{5-x} photocatalyst was obtained; the O/Nb ratio was close to the theoretical value of 2.5. In addition, according to the study of hydrogen production of bicomponent photocatalyst powders (CuO/Nb_2O_{5-x}, NiO/Nb_2O_{5-x} and Pt/Nb_2O_{5-x}) synthesized by the addition of cocatalysts using Nb_2O_{5-x} powder and undergoing thermal treatment at 500 °C as its base, the addition of CuO as the cocatalyst contributed to the maximum hydrogen production efficiency of 1405 μmol h^{-1} g^{-1}. When NiO was added as the cocatalyst, the hydrogen production efficiency dropped to 800 μmol h^{-1} g^{-1}; while the hydrogen production efficiency was only 510 μmol h^{-1} g^{-1} when Pt was added as the cocatalyst. These results can be attributed to incomplete oxidation during the methanol oxidation process. CO adsorption on a catalyst's metal surface (such as NiO or Pt) contributed to the reduced catalytic performance and hydrogen production rates.

Acknowledgments

This work was supported in part by the National Science Council (NSC) of the Republic of China, under grants NSC 100-2218-E-259-001 and NSC 101-2221-E-259-009.

References

[1] A. Fujishima, K. Honda, Nature 238 (1972) 37–38.
[2] H.Y. Lin, H.C. Huang, W.L. Wang, Microporous Mesoporous Mat. 115 (2008) 568–575.
[3] L. Berger, H. Mähne, V. Klemm, A. Leuteritz, T. Mikolajick, D. Rafaja, Appl. Phys. A 108 (2012) 431–437.
[4] T. Sreethawong, S. Ngamsinlapasathian, S. Yoshikawa, Mater. Lett. 78 (2012) 135–138.
[5] D.W. Hwang, H.G. Kim, J. Kim, K.Y. Cha, Y.G. Kim, J.S. Lee, J. Catal. 193 (2000) 40–48.
[6] A. Kudo, Catal. Surv. Asia 7 (1) (2003) 31–38.
[7] H.Y. Lin, H.C. Yang, W.L. Wang, Catal. Today 174 (2011) 106–113.
[8] N.L. Wu, M.S. Lee, Int. J. Hydrogen Energy 29 (2004) 1601–1605.
[9] H.Y. Lin, Y.S. Chang, Int. J. Hydrogen Energy 35 (2010) 8463–8471.
[10] H.Y. Lin, T.H. Lee, C.Y. Sie, Int. J. Hydrogen Energy 33 (2008) 4055–4063.
[11] Y.H. Pai, G.R. Lin, Opt. Express 19 (2) (2011) 896–905.
[12] I. Nowak, M. Ziolek, Chem. Rev. 99 (1999) 3603–3624.
[13] H. Lim, J. Choi, J. Ind. Eng. Chem. 15 (2009) 860–864.
[14] C. Koch, Rev. Adv. Mater. Sci. 5 (2003) 91–99.
[15] X.L. Duan, X.Q. Wang, F.P. Yu, D.R. Yuan, J. Phys. Chem. C 116 (2012) 2313–2321.
[16] W. Huang, J. Shi, Scripta Mater. 44 (2001) 117–123.
[17] M.K. Jeon, J.W. Park, M. Kang, J. Ind. Eng. Chem. 13 (1) (2007) 84–91.
[18] J. Chen, D.F. Ollis, W.H. Rulkens, H. Bruning, Water Res. 33 (1999) 669–676.
[19] T. Bak, J. Nowotny, M. Rekas, C.C. Sorrell, Int. J. Hydrogen Energy 27 (2002) 991.
[20] J. Yu, Y. Hai, M. Jaroniec, J. Colloid Interface Sci. 357 (1) (2011) 223–228.
[21] J. Rask, J. Bontovics, F. Solmosi, J. Catal. 146 (1) (1994) 22–27.
[22] X.Y. Jiang, R.X. Zhou, J. Yuan, G.L. Lu, X.M. Zheng, J. Rare Earth 21 (1) (2003) 55–59.
[23] A. Mishra, R. Prasad, Bull. Chem. Reac. Eng. Catal. 6 (2011) 1–14.
[24] Y. Liu, Q. Fu, M.F. Stephanopoulos, Catal. Today 93–95 (2004) 241–246.
[25] T. Santa-Nokki, H. Hakkinen, Chem. Phys. Lett. 406 (2005) 44–48.
[26] E. Wartnaby, A. Stuck, Y.Y. Yeo, D.A. King, Chem. Phys. 102 (1995) 1855.
[27] X. Zhang, K.Y. Chan, Chem. Mater. 15 (2003) 451–459.